Residual homogenization for elastic wave propagation in complex media

Yann Capdeville, Philippe Cance

Geophysical Journal International

Geophys. J. Int. (2015) **200,** 986–999
GJI Seismology

doi: 10.1093/gji/ggu452

Residual homogenization for elastic wave propagation in complex media

Yann Capdeville and Philippe Cance

Laboratoire de Planétologie et Géodynamique de Nantes, CNRS, Université de Nantes, Nantes, France. E-mail: yann.capdeville@univ-nantes.fr

Accepted 2014 November 17. Received 2014 October 23; in original form 2014 September 10

SUMMARY

In the context of elastic wave propagation, the non-periodic homogenization asymptotic method allows to find a smooth effective medium and equations that correspond to the wave propagation in a given complex elastic or acoustic medium down to a given minimum wavelength. By smoothing all discontinuities and fine scales of the original medium, the homogenization technique considerably reduces meshing difficulties as well as the numerical cost associated with the wave equation solver, while producing the same waveform as for the original medium (up to the wanted accuracy). We present here a variation of the original method, allowing to homogenize the difference, or residual, between an original medium and a reference medium. This makes it possible to, for example, homogenize some specific parts of a model or to leave unchanged a specific interface while homogenizing the rest of the model. We present two examples of applications, one implying a complex geological shallow structure and the other involving the combination of deterministic and stochastic elastic models.

Key words: Numerical solutions; Seismic anisotropy; Computational seismology; Theoretical seismology; Wave scattering and diffraction; Wave propagation.

1 INTRODUCTION

For many applications, seismologists work with limited frequency-band data of the ground motion recorded by seismic stations. This can be due to attenuation or instrument response but most of the time, it is simply the seismologist himself who limits the frequency content of his data using a bandpass filter. The reasons to do so are linked to limited computing power resources available to model the data, but also to a limited knowledge of the Earth underground. In the far-field of the source, the fact that data have a maximum frequency $f_{\max}$ ensures that the wavefield has a minimum wavelength $\lambda_{\min}$. Solving the seismic forward problem using numerical methods (such as finite differences, spectral elements, etc.), that is solving the wave equation to obtain the waveform at any space location, strongly relies on this knowledge of a $\lambda_{\min}$ to accurately sample the wavefield. To estimate the numerical cost scaling (or computing time) necessary to solve the forward problem for a fixed signal duration as a function of $\lambda_{\min}$, we need to distinguish two cases, depending on the regularity of the elastic medium in consideration. We assume that the elastic medium in which we need to solve the forward problem has a minimum heterogeneity characteristic size $\lambda_{\rm h}$. $\lambda_{\rm h}$ could be the shortest distance between two layers of a discontinuous medium or the fastest oscillation scale of a continuous medium.

(i) if $\lambda_{\rm h} \gg \lambda_{\min}$, we are in the smooth medium case. In such a case, for $N_{\rm s}$ sources, the computing time $t_{\rm c}$ scales as

$$t_{\rm c} \propto N_{\rm s}\lambda_{\min}^{-(d+1)}, \tag{1}$$

where d is the problem dimension (2-D or 3-D). This is the optimal case and this scaling can only be improved with some extra symmetries or assumptions on the medium.

(ii) if $\lambda_{\rm h} \ll \lambda_{\min}$, we are in the rough medium case. In such a case, the computing time $t_{\rm c}$ scales as

$$t_{\rm c} \propto N_{\rm s}\lambda_{\rm h}^{-(d+1)}. \tag{2}$$

This second case is very common in most realistic applications. In practice, this $\lambda_{\rm h}^{-(d+1)}$ scaling appears differently depending on the numerical solver used to solve the wave equation. For example, if finite elements are considered, then complex, fine and discontinuous structures lead to a complex mesh which is usually difficult to generate and expensive to use. Indeed, in order to be accurate, the finite element mesh needs to honour all medium discontinuities. If finite differences are used, then small structures impose an expensive oversampling of the wavefield. Case (2) is therefore a non-optimal configuration and a seismologist feels he is paying a computing price that he should not. This intuition is linked to the fact that it is well known from observations that, somehow, waves of $\lambda_{\min}$ wavelength are sensitive to small heterogeneity scales $\lambda_h \ll \lambda_{\min}$ only in an effective way and, if this effective medium was known, we could go back to the optimal scaling cost (1). This is exactly the objective of the non-periodic homogenization (Capdeville *et al.* 2010a,b; Guillot *et al.* 2010): finding the upscaling operator allowing to compute the effective medium of a given rough medium so that the numerical cost scales as $t_{\rm c} \propto N_{\rm s}\lambda_{\min}^{-(d+1)}$ even if $\lambda_{\rm h} \ll \lambda_{\min}$. The non-periodic homogenization method gets its name by opposition to the so-called two scale periodic homogenization

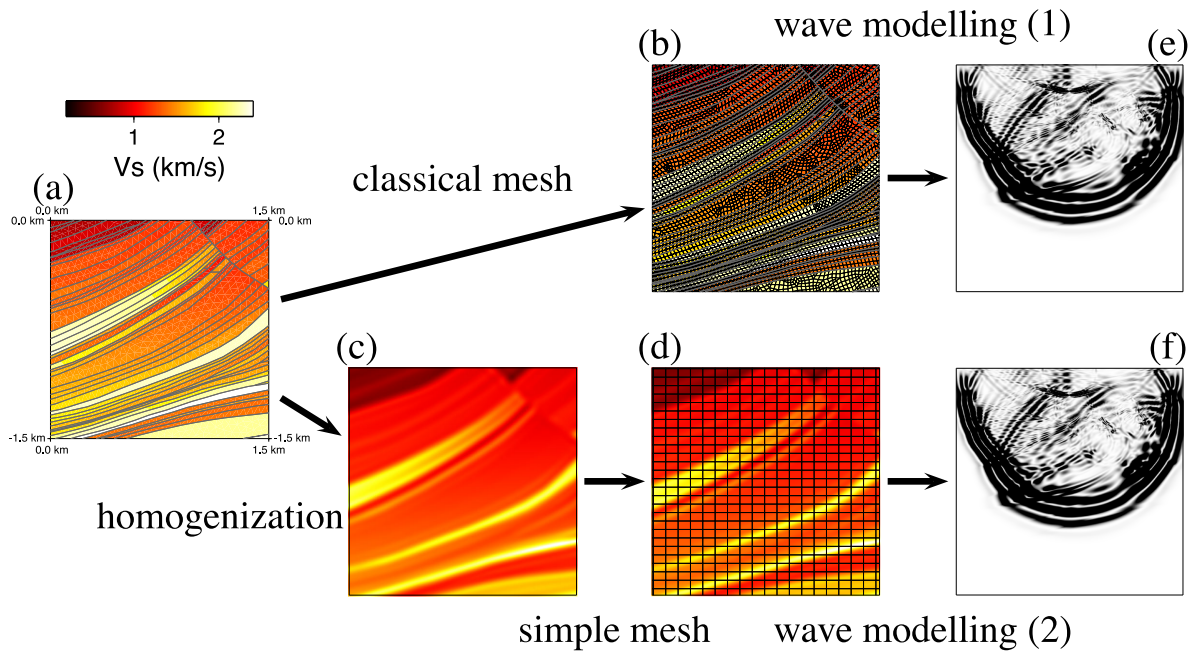

Figure 1. Homogenization principle. One wishes to propagate waves up to a maximum frequency f_{max} in a complex elastic model (a) using a numerical solver (e.g. the spectral element method). The first and classical solution is to mesh all discontinuities of (a) to obtain the complex mesh (b) (here a spectral element mesh) and then to perform the waveform modelling (1) to obtain the wavefield (e). The second option is to use homogenization to compute the effective elastic model (c) from (a) valid up to f_{max}; (c) is fully anisotropic but smooth, which leads to a simple mesh (d). Finally the waveform modelling (2) is performed with the same numerical solver as the one used for waveform modelling (1) to obtain the wavefield (f), but at a lower numerical cost than (e). For a small enough ε_0 (see text), (f) converges to (e). The homogenization of this particular example (the Marmousi model) is detailed in Capdeville *et al.* (2010b).

(Sanchez-Palencia 1980) from which it is derived, a very powerful method but limited to periodic media. A sketch summarizing the non-periodic homogenization principle in the forward modelling context is shown in Fig. 1. The main idea of the method is to compute an effective version of the original medium for which meshing and waveform computation are simpler and cheaper without degrading the waveform accuracy. It can be seen as a pre-processing step applied to the medium before importing it into the wave equation solver. It can also be seen as a generalization of the Backus averaging (or upscaling) technique (Backus 1962). Once the homogenized medium is obtained, any wave equation solver can be used, as long as it can handle fully anisotropic and continuously varying media.

So far, we have justified the homogenization in the forward modelling context, but one could have done it for the full waveform inverse problem context as well. Indeed, homogenization is very useful to build an inverse problem based on a multiscale parameterization (Capdeville *et al.* 2013) and is already used to simplify the difficulties linked to the Earth heterogeneous crust (Capdeville & Marigo 2008; Fichtner & Igel 2008; Lekić *et al.* 2010) or to combine inverted models from different scales (Fichtner *et al.* 2013).

In this paper, we introduce a slightly more general homogenization technique that we name the residual homogenization, which principle has already been presented in Capdeville & Marigo (2013) for the layered media case. We present here the higher dimension case which, as usual for homogenization problems, is significantly more complex than the one dimension case. The residual homogenization makes it possible to homogenize the difference between two models, a target model and a reference model. The target model is the 'real' elastic model, the one in which we need to model wave propagation. The reference model is an elastic model chosen by the user, for example, for its simplicity. If the reference model is a constant model, then the residual homogenization falls back to the classical homogenization. If the reference model is equal to the target model then the homogenized model is simply the target model. However usually the reference model is chosen to make it possible to homogenize only a precise part of the target model, where the target model and the reference models are different. For example, if for a crustal model, one wants to homogenize everything but the Moho interface, then the reference model is a two layers model with the Moho interface in it. The residual homogenization is not only useful to solve meshing problems of the forward problem and it can also be used to combine two models of different scales as it will be shown in the examples section. Finally, one of the most promising aspect of the residual homogenization is for the inverse problem: we expect a full waveform inversion carried out in a limited frequency band to obtain, at best, the residual homogenized model between the real model and the reference model used for the inversion. This conjecture has been shown to be numerically true in the layered case (Capdeville & Marigo 2013) but this remains to be shown for higher dimension cases.

The paper is organized as follows: we first briefly remind the principle of the non periodic homogenization. We then introduce the residual homogenization. Two examples of application in 2-D are then given, first a forward modelling example and then a model combining example.

2 THE HOMOGENIZATION ALGORITHM TO OBTAIN THE EFFECTIVE ELASTIC TENSOR AS WELL AS SOURCE AND RECEIVER CORRECTORS

We give here a summary of the technique described in Capdeville *et al.* (2010a,b) and Guillot *et al.* (2010). A reader interested in a

more detailed and self-consistent justification of the method should refer to these articles.

In the following, we assume that the seismic source $\boldsymbol{f}(\mathbf{x}, t)$ is such that it has a maximum frequency $f_{\max}$, making sure that, in the far-field, the wavefield has a minimum wavelength $\lambda_{\min}$. For a given elastic medium described by its density and elastic tensor $(\rho, \mathbf{c})$ at any point $\mathbf{x}$ of the physical domain $\boldsymbol{\Omega}$, we consider the elastodynamic problem in $\boldsymbol{\Omega}$:

$$\rho \partial_{tt} \mathbf{u} - \boldsymbol{\nabla} \cdot \boldsymbol{\sigma} = \boldsymbol{f}, \tag{3}$$

$$\boldsymbol{\sigma} = \mathbf{c} : \boldsymbol{\epsilon}(\mathbf{u}), \tag{4}$$

associated with the appropriate boundary conditions on $\partial\boldsymbol{\Omega}$, where $\mathbf{u}(\mathbf{x}, t)$ is the displacement field for $t \in [0, T]$, T the signal duration, $\boldsymbol{\sigma}(\mathbf{x}, t)$ the stress, $\boldsymbol{\epsilon}(\mathbf{u}) = \frac{1}{2}(\boldsymbol{\nabla}\mathbf{u} + {}^T\boldsymbol{\nabla}\mathbf{u})$ the strain and ^{T} the transpose operator. The homogenization technique, at the order 0, aims to approximate the above original problem with the following effective equations:

$$\rho^{\varepsilon_0} \partial_{tt} \mathbf{u}^{\varepsilon_0} - \boldsymbol{\nabla} \cdot \boldsymbol{\sigma}^{\varepsilon_0} = \boldsymbol{f}, \tag{5}$$

$$\boldsymbol{\sigma}^{\varepsilon_0} = \mathbf{c}^{\varepsilon_0} : \boldsymbol{\epsilon}(\mathbf{u}^{\varepsilon_0}), \tag{6}$$

still with the appropriate boundary conditions on $\partial\boldsymbol{\Omega}$ (at the order 0, the boundary conditions do not change from the original problem), where $(\rho^{\varepsilon_0}, \mathbf{c}^{\varepsilon_0})$ are the ε_0 effective density and elastic parameters, $\mathbf{u}^{\varepsilon_0}(\mathbf{x}, t)$ the order 0 homogenized displacement and $\boldsymbol{\sigma}^{\varepsilon_0}(\mathbf{x}, t)$ the average of the order 0 homogenized stress. The ε_0 parameter is a user defined parameter which controls the level of details of the effective medium with respect to $\lambda_{\min}$:

$$\varepsilon_0 = \frac{\lambda_0}{\lambda_{\min}}. \tag{7}$$

λ_0 defines the value below which all scales are considered as small scales (also named 'fast scales' or microscopic scales) and above which all scales are considered as large scales (also named 'slow scales' or macroscopic scales). With hand waving, an $\varepsilon_0 < 1$ means that the effective solutions will keep more details than $\lambda_{\min}$ in the elastic model description, and $\varepsilon_0 > 1$ means that it will be smoother than $\lambda_{\min}$. In practice, for most geophysical applications, having ε_0 lying between 0.25 and 0.5 is often a good choice, but it all depends on the wanted accuracy, on the signal duration and on the particular elastic model in consideration. The only point guaranteed by the method is the convergence rate with ε_0 (see below).

To the order 1, the relation between the true displacement $\mathbf{u}$ and the homogenized displacement $\mathbf{u}^{\varepsilon_0}$ is:

$$\mathbf{u}(\mathbf{x}, t) = \mathbf{u}^{\varepsilon_0}(\mathbf{x}, t) + \varepsilon_0 \boldsymbol{\chi}^{\varepsilon_0}(\mathbf{x}, \mathbf{x}/\varepsilon_0) : \boldsymbol{\epsilon}(\mathbf{u}^{\varepsilon_0})(\mathbf{x}, t) + O(\varepsilon_0), \tag{8}$$

where $\boldsymbol{\chi}^{\varepsilon_0}(\mathbf{x}, \mathbf{y})$ is the first order corrector and accounts for the site effect. $\boldsymbol{\chi}^{\varepsilon_0}$ depends on two independent space variables: the regular space position $\mathbf{x}$ and on the microscopic scale variable $\mathbf{y}$. In practice, the only useful value for the fast scale variable is $\mathbf{y} = \mathbf{x}/\varepsilon_0$. This two variables formulation is an important aspect of the two scale homogenization theory and one can refer to, for example, Sanchez-Palencia (1980) for a deeper explanation. In practice, (8) is often valid in $O(\varepsilon_0^2)$ (see Capdeville *et al.* 2010a). Similarly, we have:

$$\boldsymbol{\sigma}(\mathbf{x}, t) = \mathbf{H}^{\varepsilon_0}(\mathbf{x}, \mathbf{x}/\varepsilon_0) : \boldsymbol{\epsilon}\left(\mathbf{u}^{\varepsilon_0}\right)(\mathbf{x}, t) + O(\varepsilon_0), \tag{9}$$

$$\boldsymbol{\epsilon}(\mathbf{x}, t) = \mathbf{G}^{\varepsilon_0}(\mathbf{x}, \mathbf{x}/\varepsilon_0) : \boldsymbol{\epsilon}\left(\mathbf{u}^{\varepsilon_0}\right)(\mathbf{x}, t) + O(\varepsilon_0), \tag{10}$$

where $\mathbf{H}^{\varepsilon_0}(\mathbf{x}, \mathbf{y})$ and $\mathbf{G}^{\varepsilon_0}(\mathbf{x}, \mathbf{y})$ are the stress and strain concentrators and are also linked to site effects. Computing $(\rho^{\varepsilon_0}, \mathbf{c}^{\varepsilon_0})$ as well as $\boldsymbol{\chi}^{\varepsilon_0}$, $\mathbf{H}^{\varepsilon_0}$ and $\mathbf{G}^{\varepsilon_0}$ for non-periodic media is the main contribution of Capdeville *et al.*'s (2010a,b) and Guillot *et al.*'s (2010) work.

Before moving forward into the description of the method, we need to introduce a low-pass filter operator $\mathcal{F}^{k_0}$, such that, for any quantity $g(\mathbf{x})$, $\mathcal{F}^{k_0}(g)(\mathbf{x})$ does not contain any spatial variation faster than $\lambda_0 = 2\pi/k_0$. This low-pass filter operator can be written as:

$$\mathcal{F}^{k_0}(g)(\mathbf{x}) = (w^{k_0} * g)(\mathbf{x}), \tag{11}$$

where $*$ is the spatial convolution and w^{k_0} is the filter wavelet.

The effective medium and correctors are obtained the following way:

Step 1: We first solve the so-called cell problem to find the initial guess correctors $\boldsymbol{\chi}_{\mathrm{s}}^{lm}(\mathbf{x})$. It consists in solving the following elastostatic set of problems (3 in 2-D, 6 in 3-D) in $\boldsymbol{\Omega}$:

$$\begin{aligned} \boldsymbol{\nabla} \cdot \mathbf{c} : \boldsymbol{\epsilon}\left(\boldsymbol{\chi}_{\mathrm{s}}^{lm}\right) &= \mathbf{F}^{lm}, \\ \mathbf{F}^{lm} &= -\boldsymbol{\nabla} \cdot [\mathbf{c} : (\mathbf{e}_l \otimes \mathbf{e}_m)] \end{aligned} \tag{12}$$

for $(l, m) \in \{1..d\}^2$, with periodic boundary conditions on $\partial\Omega$. This first step is a fine scale problem to be solved on the whole domain and is therefore usually numerically expensive. Two methods are currently available to solve (12), one based on a finite element solver (Capdeville *et al.* 2010b) and one based on a fast Fourier iterative scheme (Capdeville *et al.* 2014).

Step 2: Once the initial corrector guess $\boldsymbol{\chi}_{\mathrm{s}}^{lm}$ is obtained, we compute:

$$\begin{aligned} [\mathbf{G}_{\mathrm{s}}]_{ijlm}(\mathbf{x}) &= \frac{1}{2}\left(\delta_{il}\delta_{jm} + \delta_{jl}\delta_{im}\right) + \left[\boldsymbol{\epsilon}\left(\boldsymbol{\chi}_{\mathrm{s}}^{lm}\right)\right]_{ij}, \\ \mathbf{H}_{\mathrm{s}}(\mathbf{x}) &= \mathbf{c} : \mathbf{G}_{\mathrm{s}}. \end{aligned} \tag{13}$$

The ε_0 effective elastic tensor can be directly obtained as:

$$\mathbf{c}^{\varepsilon_0}(\mathbf{x}) = \mathcal{F}^{k_0}(\mathbf{H}_{\mathrm{s}}) : \mathcal{F}^{k_0}(\mathbf{G}_{\mathrm{s}})^{-1}(\mathbf{x}). \tag{14}$$

The effective density is simply:

$$\rho^{\varepsilon_0}(\mathbf{x}) = \mathcal{F}^{k_0}(\rho)(\mathbf{x}). \tag{15}$$

Step 3: Finally, the stress and strain concentrators are obtained as:

$$\begin{aligned} \mathbf{G}^{\varepsilon_0}(\mathbf{x}, \mathbf{y}) &= \left(\mathcal{F}^{k_0}(\mathbf{G}_{\mathrm{s}})(\mathbf{x}) + \left(\mathbf{G}_{\mathrm{s}} - \mathcal{F}^{k_0}(\mathbf{G}_{\mathrm{s}})\right)(\varepsilon_0 \mathbf{y})\right) : \mathcal{F}^{k_0}(\mathbf{G}_{\mathrm{s}})^{-1}(\mathbf{x}), \\ \mathbf{H}^{\varepsilon_0}(\mathbf{x}, \mathbf{y}) &= \left(\mathcal{F}^{k_0}(\mathbf{H}_{\mathrm{s}})(\mathbf{x}) + \left(\mathbf{H}_{\mathrm{s}} - \mathcal{F}^{k_0}(\mathbf{H}_{\mathrm{s}})\right)(\varepsilon_0 \mathbf{y})\right) : \mathcal{F}^{k_0}(\mathbf{G}_{\mathrm{s}})^{-1}(\mathbf{x}), \end{aligned} \tag{16}$$

and the first order corrector $\boldsymbol{\chi}^{\varepsilon_0}(\mathbf{x}, \mathbf{y})$ is obtained solving, for each $\mathbf{x}$ (fixed):

$$\boldsymbol{\nabla}\boldsymbol{\chi}^{\varepsilon_0}(\mathbf{x}, \mathbf{y}) + {}^T\boldsymbol{\nabla}\boldsymbol{\chi}^{\varepsilon_0}(\mathbf{x}, \mathbf{y}) = 2(\mathbf{G}^{\varepsilon_0}(\mathbf{x}, \mathbf{y}) - \mathbf{I}), \tag{17}$$

where the $\boldsymbol{\nabla}$ operators here applies on the $\mathbf{y}$ variable and $\mathbf{I}$ is the identity operator.

As often with homogenization techniques, the physical interpretations of the steps 1–3 are not obvious. This process to compute the effective elastic properties can be linked to a heuristic approach to obtain an effective elastic tensor by computing the average stresses and strains associated with a set of elementary static problems and finding the average tensor linking them [this approach is known as the average method (Suquet 1982)]. In step 1, the elastic domain is statically loaded with a set of forces $\mathbf{F}^{lm}$, making it possible to obtain a corresponding set of strain tensors $\boldsymbol{\epsilon}(\boldsymbol{\chi}_{\mathrm{s}}^{lm})$. The set of forces is such that it allows to fully characterize the system. In step 2, from the set of strain tensors obtained in step 1, two tensors $\mathbf{G}_{\mathrm{s}}$ and $\mathbf{H}_{\mathrm{s}}$, which can be related, respectively, to sets of strain and stress tensors, are

built. The effective tensor is the one linking all the possible stress ($\mathbf{H}_s$) and strain ($\mathbf{G}_s$) tensors at the 'wave scale'. The 'wave scale' means that we assume that the wavefield is not oscillating faster than a wavenumber k_0 and that all scales oscillating faster than k_0 are smoothed by the wave. This is what is done in (14): the sets of strain and stress tensors characterizing the medium are smoothed to the wave scale using the low-pass filter $\mathcal{F}^{k_0}$, to obtain effective sets of strain and stress tensors. The effective tensor is what relates these two smoothed sets of tensor. In this process, the relation with the wave equation is made through the filter $\mathcal{F}^{k_0}$: it is smoothing the stress and strain tensors as the wave would, in a conservative way (the actual waves may smooth further the tensors than the low-pass filter). In step 3, the stress and strain concentrators are computed. The idea is here, using the low past filter again, to assign the slow scales to the slow space variable $\mathbf{x}$ and the fast scales to the fast space variable $\mathbf{y}$.

At this stage, everything is ready: the effective medium is known and can be used in our favourite wave equation solver, as long it can handle anisotropy and continuously varying media, to obtain the order 0 effective displacement $\mathbf{u}^{\varepsilon_0}$. If necessary, the order 0 displacement can *a posteriori* be corrected from local site effect applying (8). Because the effective medium is smooth, the mesh design (for finite element method solver type) or sampling (for finite differences method solver type) is very simple. Nevertheless, because the effective medium is oscillating usually faster than the wavefield, compared to the classical sampling in smooth media, an oversampling linked to ε_0 is necessary. In practice, we use the following rule of thumb:

$$\Delta^{\varepsilon_0} = \frac{\Delta}{1 + \frac{1}{2\varepsilon_0}}, \tag{18}$$

where Δ is the one-direction space sampling or element size computed in a locally homogeneous media and Δ^{ε_0} the actual sampling or element size that has to be used to account for the effective medium oscillations. As a result, the smallest is ε_0, the finer the sampling has to be (leading to a higher numerical cost for the solver). This can be a problem if for some reasons ε_0 has to be very small to achieve the wanted accuracy, and this is one of the motivation for the residual homogenization presented here as it will be seen with the first application example presented in Section 4.1.

Once the effective wavefield is computed, the local effect operators are also ready to be applied to the output of the wave equation solver. The efficiency of the non-periodic homogenization summarized here has been demonstrated in, for example, Capdeville *et al.* (2010b) and we do not propose any new validation of the method here.

Finally, let us mention that nothing has been said about the boundary conditions on the original problem (like the Neumann condition at the free surface), which should not be confused with the boundary conditions of the cell problem, and how they can be modified by the homogenization process. Beyond the order 0, they usually deserve a special treatment as described in Capdeville & Marigo (2008, 2013).

3 RESIDUAL HOMOGENIZATION

We now introduce two elastic models:

(i) $(\rho^0, \mathbf{c}^0)$, the reference model;
(ii) $(\rho, \mathbf{c})$, the target model.

The target model is the same model as for the previous section. It is the 'real' model, the one in which we need to model the wavefield. The reference model is a user defined model. Its design is up to the user without any specific restrictions. In particular, it can contain small scales that, for some reason, the user does not wish to homogenize.

If the models are layered, because an analytical solution to the cell problem (12) exists, designing a residual homogenization process is simple as shown by Capdeville *et al.* (2013). In such a case, it appears that the residual effective medium can simply be obtained by smoothing the residual of the Backus parameters. The Backus parameters are built upon a non-linear combination of the A, C, F, L, N elastic parameters necessary to describe a vertically transverse isotropic medium (Takeuchi & Saito 1972). The Backus parameters are the parameters that should be averaged for a proper upscaling in a layered medium (Backus 1962). For example, one of these parameter is $1/C$ (see Backus 1962 or Capdeville *et al.* 2013 for a complete list of the Backus parameters). For this particular Backus parameter, the classical effective C^{ε_0} is simply obtained as:

$$\frac{1}{C^{\varepsilon_0}} = \mathcal{F}^{k_0}\left(\frac{1}{C}\right), \tag{19}$$

whereas the residual effective C^{ε_0} with respect to the reference C^0 is obtained as:

$$\frac{1}{C^{\varepsilon_0}} = \frac{1}{C^0} + \mathcal{F}^{k_0}\left(\frac{1}{C} - \frac{1}{C^0}\right). \tag{20}$$

It can be seen in the last expression that only the residual between the target and reference Backus parameters is low-pass filtered, implying that the small scales present in $1/C^0$ are not smoothed and still present in $1/C^{\varepsilon_0}$.

Unfortunately, no such analytical solution exists for higher dimension problems, and we cannot use the layered case simple solution anymore. For higher dimension problems, we have to work on the $\mathbf{G}_s$ and $\mathbf{H}_s$ tensors (13), derived from the solutions of the cell problem. Based on the reference and target models, the homogenization procedure presented in the previous section is modified to obtain:

Step 1: The cell problem (12) is solved twice, once for the reference model and once for the target model, and two initial corrector guesses are found.

Step 2: From (13), we obtain two sets of initial stress and strain concentrators:

(1) $(\mathbf{G}_s^0, \mathbf{H}_s^0)$ for the reference model;
(2) $(\mathbf{G}_s, \mathbf{H}_s)$ for the target model.

Setting:

$$\begin{aligned}
\delta\mathbf{G}_s(\mathbf{x}) &= \mathbf{G}_s(\mathbf{x}) - \mathbf{G}_s^0(\mathbf{x}),\\
\delta\mathbf{H}_s(\mathbf{x}) &= \mathbf{H}_s(\mathbf{x}) - \mathbf{H}_s^0(\mathbf{x}),\\
\delta\rho(\mathbf{x}) &= \rho(\mathbf{x}) - \rho^0(\mathbf{x}),
\end{aligned} \tag{21}$$

the ε_0 residual homogenized model is directly obtained as:

$$\mathbf{c}^{\varepsilon_0}(\mathbf{x}) = \left(\mathbf{H}_s^0 + \mathcal{F}^{k_0}(\delta\mathbf{H}_s)\right) : \left(\mathbf{G}_s^0 + \mathcal{F}^{k_0}(\delta\mathbf{G}_s)\right)^{-1}(\mathbf{x}). \tag{22}$$

The effective density is simply:

$$\rho^{\varepsilon_0}(\mathbf{x}) = \rho^0(\mathbf{x}) + \mathcal{F}^{k_0}(\delta\rho)(\mathbf{x}). \tag{23}$$

Step 3: Finally, the stress and strain concentrators are obtained as:

$$\mathbf{G}^{\varepsilon_0}(\mathbf{x},\mathbf{y}) = \left(\mathbf{G}_s^0(\mathbf{x}) + \mathcal{F}^{k_0}(\delta\mathbf{G}_s)(\mathbf{x}) + \left(\delta\mathbf{G}_s - \mathcal{F}^{k_0}(\delta\mathbf{G}_s)\right)(\varepsilon_0\mathbf{y})\right) : \left(\mathbf{G}_s^0(\mathbf{x}) + \mathcal{F}^{k_0}(\delta\mathbf{G}_s)(\mathbf{x})\right)^{-1},$$

$$\mathbf{H}^{\varepsilon_0}(\mathbf{x},\mathbf{y}) = \left(\mathbf{H}_s^0(\mathbf{x}) + \mathcal{F}^{k_0}(\delta\mathbf{H}_s)(\mathbf{x}) + \left(\delta\mathbf{H}_s - \mathcal{F}^{k_0}(\delta\mathbf{H}_s)\right)(\varepsilon_0\mathbf{y})\right) : \left(\mathbf{G}_s^0(\mathbf{x}) + \mathcal{F}^{k_0}(\delta\mathbf{G}_s)(\mathbf{x})\right)^{-1}, \quad (24)$$

and the first order corrector $\boldsymbol{\chi}^{\varepsilon_0}(\mathbf{x},\mathbf{y})$ is obtained solving (17).

Once again the above procedure is not straightforward to interpret. Again, the idea is that the tensors $\mathbf{G}_s$ and $\mathbf{H}_s$ fully characterize the elastic medium and that the wanted effective tensor relates the smoothed version of these two tensors. In the residual homogenization case, two media are used, a reference and a target media. To these two media correspond two sets of tensors: $(\mathbf{G}_s^0, \mathbf{H}_s^0)$ for the reference model and $(\mathbf{G}_s, \mathbf{H}_s)$ for the target model. In order to keep the details from the reference model to the effective medium, only the residual of the $\mathbf{G}_s$ and $\mathbf{H}_s$, defined in (21), are smoothed. The residual homogenized model can only be interpreted as the media 'seen' by the wavefield if the reference model is smooth. If the reference model is rough, an interpretation can be found in the full waveform inversion problem: we expect that a full waveform inversion starting from a rough reference model can , at best, obtain the residual homogenized model between and real model and the reference model. This has been numerically shown in the layered case (Capdeville *et al.* 2013).

In the layered case, it can be checked that this procedure is strictly equivalent to the explicit formula obtained in Capdeville *et al.* (2013). Moreover, it can be checked that, following this procedure, all the necessary criteria to obtain the corrector and solutions in the appropriate solution space are fulfilled (see Capdeville *et al.* 2010b), allowing to obtain the same convergence rate as for (8). This means that, with respect to the convergence rate with ε_0 nothing has been gained, but the constant factor of the $O(\varepsilon_0)$ has been changed, which in practice can be a significant advantage as it will be shown in the first application example.

4 APPLICATION EXAMPLES

To illustrate the capabilities of the residual homogenization, we give here two application examples. The first one is a typical forward modelling application where meshing and numerical cost are the issues to be solved. The second example is also a forward modelling example in a case where reducing the numerical cost is not the objective, but where the difficulty lies in combining properly two different elastic models of different scale contents.

In the following, the spectral element method (Komatitsch & Vilotte 1998; Chaljub *et al.* 2007) is used to solve the reference and homogenized wave equations. Perfectly matched layers (PMLs) absorbing boundary conditions are used where necessary [Festa & Vilotte's (2005) version].

4.1 Rayleigh wave and a shallow slow layer

In this section, our objective is to compute the wavefield in the target model given in Figs 2 and 3. It is a complex 2-D elastic model, with a thin shallow slow layer (100 m thick) and with two tilted layered area merging with the slow layer close to the free surface. This model is not intended to be a realistic geological model, but rather a model that partly mimic the complexity of a realistic situation that could occur in sediment basin for example. Assuming that the minimum wavelength of the wavefield we need to propagate in this elastic model is about 1 km, the difficulties are due to the fine structures in the tilted thin layers (140 m of periodicity) and especially where these layers merge with the shallow slow layer. Indeed, this complex area leads to a fine and complex mesh, implying a high numerical cost for the spectral element solver. Such a mesh is possible to generate in 2-D, but would be extremely difficult to generate in 3-D similar case.

The source time function used is a Ricker (second derivative of a Gaussian) of central frequency 1.1 Hz leading to a maximum frequency of about 3.2 Hz and an estimate of the minimum wavelength of 1 km in the background medium [material (0) in Fig. 2 and Table 1]. On one hand, using a degree 5 for the spectral element polynomial approximation, an accurate sampling of the wavefield can be achieved using about one element per minimum wavelength

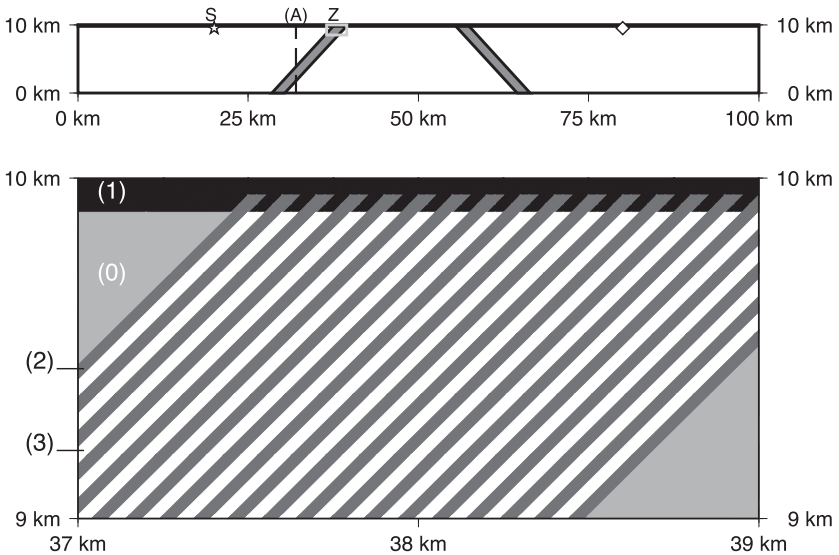

Figure 2. Top panel: sketch describing the target model used in Section 4.1. The star symbol ('S') is the source location and the diamond symbol a receiver location. The 'Z' rectangle is the zoom area displayed below and the '(A)' dashed line locates the model cross-section given in Fig. 3. Bottom panel: zoom in the 'Z' area. The model is made of four different materials [numbers (0)–(3)] given in Table 1.

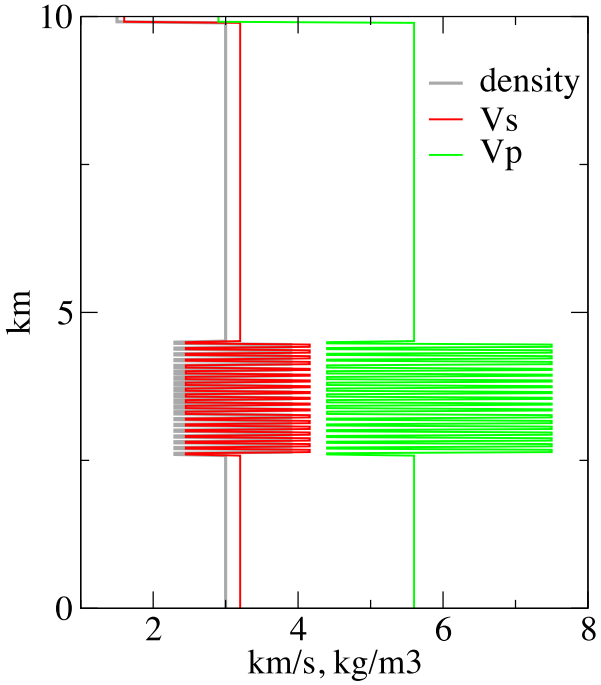

Figure 3. Section 4.1 target model vertical cross-section. The cross-section location is displayed in Fig. 2 [dashed line '(A)'].

Table 1. Material properties list used in Section 4.1.

Material number	V_P (km s^{-1})	V_S (km s^{-1})	ρ (kg m^{-3})
(0)	5.6	3.2	3000
(1)	2.9	1.6	1500
(2)	4.4	2.45	2300
(3)	7.5	4.1	3900

and therefore an element size of 1×1 km^2. On the other hand, each material discontinuity has to be meshed, whatever the minimum wavelength is. With those constraints, the mesh generator [Gmsh (Geuzaine & Remacle 2009) has been used here] does its best and a sample of the obtained mesh for the target model is shown in Fig. 4(top plot). As it can be seen, the mesh is strongly distorted, with small elements, leading to a small time step to satisfy the so-called CFL stability condition, and therefore to a high numerical cost for the spectral element solver.

As explained in the introduction, by removing the small scales from the model, the homogenization technique summarized in Section 2 can reduce the meshing and the associated numerical cost difficulties. We apply the classical homogenization technique to the target model and the obtained model, for $\varepsilon_0 = 0.5$, is shown in Fig. 5. Because the homogenization procedure requires elastic tensor and density values above the free surface, we use a symmetric extension of the model with respect to the free surface, as proposed by Capdeville & Marigo (2007). As usual with homogenization, the obtained effective media if fully anisotropic. To represent the effective medium, we first find the closest isotropic medium $(\rho^{\varepsilon_0}, \mathbf{c}^{\varepsilon_0}_{\rm iso})$ to $(\rho^{\varepsilon_0}, \mathbf{c}^{\varepsilon_0})$, following the projection method of Browaeys & Chevrot (2004). From $\mathbf{c}^{\varepsilon_0}_{\rm iso}$, an isotropic S velocity can be deduced and the amount of anisotropy is measured as $\|\mathbf{c}^{\varepsilon_0} - \mathbf{c}^{\varepsilon_0}_{\rm iso}\|/\|\mathbf{c}^{\varepsilon_0}\|$, where the matrix norm is described in Browaeys & Chevrot (2004). Fig. 5 shows the isotropic S velocity $V_S^{\rm iso}$ and the measurement of the anisotropy. It can be noticed that the shallow slow layer induces a significant amount of anisotropy below the free surface.

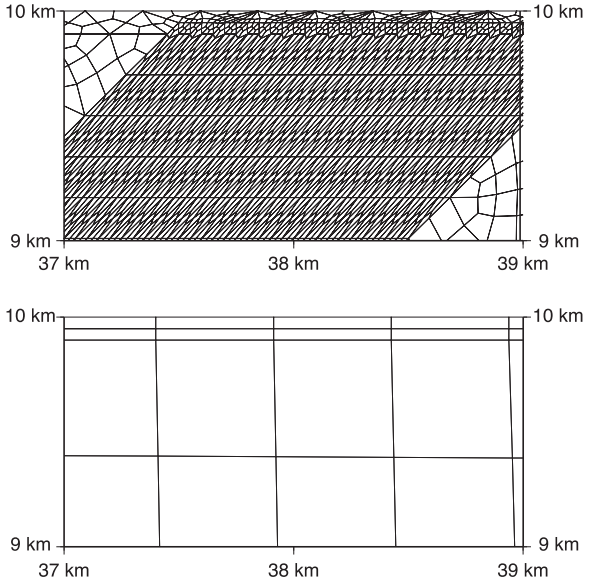

Figure 4. Top panel: sample of the spectral element mesh generated by Gmsh for the target model example of Section 4.1. Bottom panel: sample of the spectral element mesh generated by Gmsh for the reference model.

Once obtained, the effective medium $(\rho^{\varepsilon_0}, \mathbf{c}^{\varepsilon_0})$ can be used in our spectral element solver to model the wavefield. Compared to the target model case, the mesh design for the homogenized model is simple: as no material discontinuity exist anymore, we can just rely on a regular spectral element mesh, which partly fixes the small time step problem imposed by the original mesh. Nevertheless, as mentioned in the introduction, to sample correctly both the wavefield and the effective medium, the mesh element size must decrease with ε_0 (the smallest ε_0, the smallest are the elements, see eq. 18), leading to an higher numerical cost. In our previous homogenization experiments (Capdeville *et al.* 2010b), this link between the element size and ε_0 was not a problem as a good accuracy was obtained with a relatively large ε_0 (typically, $\varepsilon_0 \simeq 0.5$). The present example is different as it can be seen on seismograms (see Figs 6 and 7) recorded at the free surface, 60 km away from the source, mainly for the surface wave. Indeed, similarly to what has been observed in our previous works (Capdeville *et al.* 2010b), the first arrivals (body waves) are modelled with accuracy already with $\varepsilon_0 \simeq 0.5$, but surface waves are strongly time-shifted. This phase shift occurs because the Rayleigh wave propagates for a very long distance in the area close to the free surface, strongly affected by the homogenization. This makes it possible for the error to accumulate and to be clearly visible after a long propagation distance. Note that this strong error does not challenge the homogenization theory itself: indeed the convergence of the error to zero with ε_0 is still as expected (Fig. 10). But in practice, an unusually small ε_0 is required to achieve a good accuracy for the Rayleigh wave far away from the source, as it can be seen in Fig. 7. Indeed, $\varepsilon_0 \simeq 0.1$ is necessary to achieve a good match (a few per cent of error). Having to use a very small ε_0 is not a problem at the homogenization stage, but, as explained earlier, it imposes a finer spectral element mesh and therefore a numerical cost higher than expected for the wave equation solver.

To mitigate this technical issue, the residual homogenization presented in Section 3 is useful. We introduce a reference model (which should not be confused with the target model in which the reference solution is computed) in Fig. 8. The reference model has the same slow layer as the target model. In the regions where the tilted

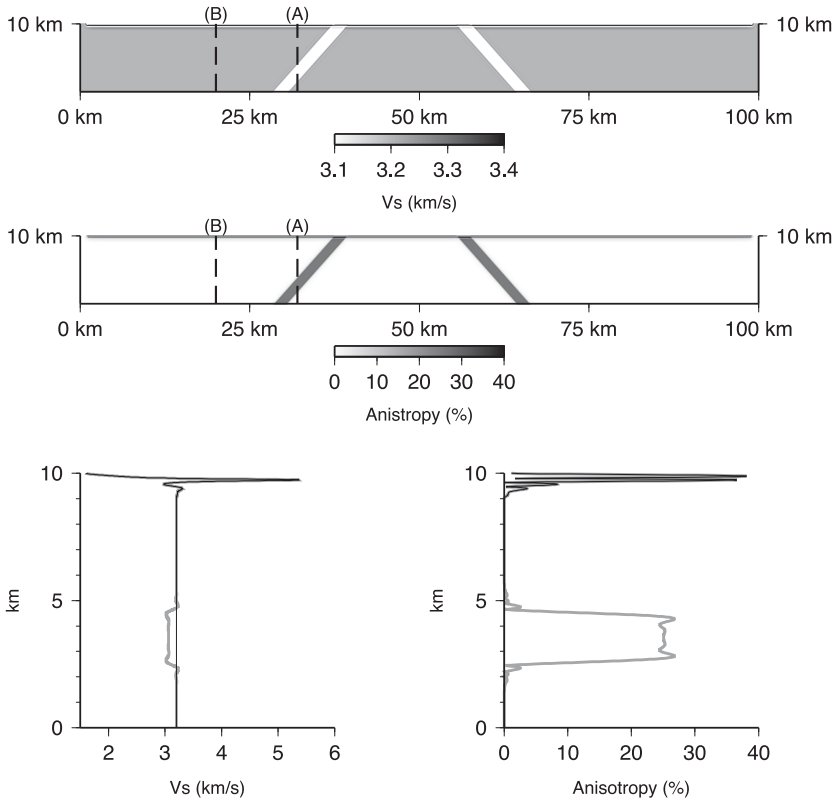

Figure 5. Effective medium obtained by homogenizing the target model shown in Fig. 2 for $\varepsilon_0 = 0.5$. The two top plots show the isotropic V_S and the amount of anisotropy in the effective medium (see text). The two bottom graphs show cross-sections (A) (grey thick lines) and (B) (black thin lines) for the isotropic V_S and the amount of anisotropy measurement.

layers merge with the slow shallow layer (in the target model), the reference model is still a constant layer but with properties representative of the average values in this complex area. The residual homogenization between the target model (Fig. 2) and the reference model (Fig. 8) is computed and the result is shown in Fig. 9. Compared to the classical homogenization results (Fig. 5), the obtained residual homogenized model is very different near the free surface: no significant homogenization effect can be observed and the original shallow discontinuity is still there. This is the main interest of the residual homogenization in such a case: it allows to choose which area should be homogenized and which should not. As a result, even for long distance wave propagation, the surface wave interaction with the area where homogenization has a strong effect is short (and actually, for this particular case, it is independent of the propagation distance, as long as the tilted layers are between the source and the receiver). As it can be seen in Figs 6 and 7, the seismograms computed in the residual homogenized model are accurate even for relatively large ε_0 (typically $\varepsilon_0 = 0.5$ here). In Fig. 6 is also plotted for comparison, the solution obtained by applying the low-pass filter to the density and the slowness, which is a naive way to obtain an effective medium. As usual, this naive upscaling achieves a poor quality result, even for the body P wave.

More qualitatively, we measure the convergence of the error, for this particular example, of the classical homogenization technique and of the residual homogenization (Fig. 10). The error is measured as:

$$E(\dot{\mathbf{u}}) = \sum_{i=1,40} \frac{\sqrt{\int_0^{t_{\max}} (\dot{\mathbf{u}} - \dot{\mathbf{u}}^{\mathrm{ref}})^2(\mathbf{x}_i, t)\mathrm{d}t}}{\sqrt{\int_0^{t_{\max}} (\dot{\mathbf{u}}^{\mathrm{ref}})^2(\mathbf{x}_i, t)\mathrm{d}t}}, \tag{25}$$

where the $\mathbf{x}_i, i \in \{1, 60\}$ are the coordinates of a set of 60 receivers located at the free surface, spaced every 1 km after the source and where $\dot{\mathbf{u}}^{\mathrm{ref}}$ is the velocity solution obtained in the target model. It can be noted in Fig. 10, that, compared to our previous work (Capdeville *et al.* 2010b) where the free boundary is not considered, we do not find a convergence in ε_0^2 but only a convergence in ε_0 (approximately). To obtain a convergence in ε_0^2, the free surface corrector (Capdeville & Marigo 2008, 2013) should have been used, which is not the case here. In Fig. 10, it can be seen that both classical homogenization and residual homogenization converge in ε_0, which is expected. If the slope of both convergence curves are similar, the residual homogenization shows a much lower error.

From the meshing point of view, the residual homogenization has an extra constraint compared to classical homogenization: the reference model has to be meshed. In this particular case, the slow layer interface must correspond to a mesh interface, as it can be seen in Fig. 4(bottom plot). We have used once again Gmsh to generate the mesh even if, in that case, a better quality mesh could have been generated manually (there is no need for two elements vertically in the slow layer). Nevertheless, to produce a fair comparison between the different possible solutions to compute the wavefield, we fully rely on Gmsh in both cases. Having to mesh the reference model is a constraint, imposing to have locally thinner elements than one could hope for a classical homogenization with the same ε_0. Nevertheless, this constraint is weaker than imposing a very small ε_0 everywhere in the model to achieve a good accuracy. About the computing performance, using the same hardware, for this particular example and for $\varepsilon_0 = 0.5$, the spectral element run to compute the solution in residual homogenized model is 40 times faster than the reference run (in the target model). For this specific example,

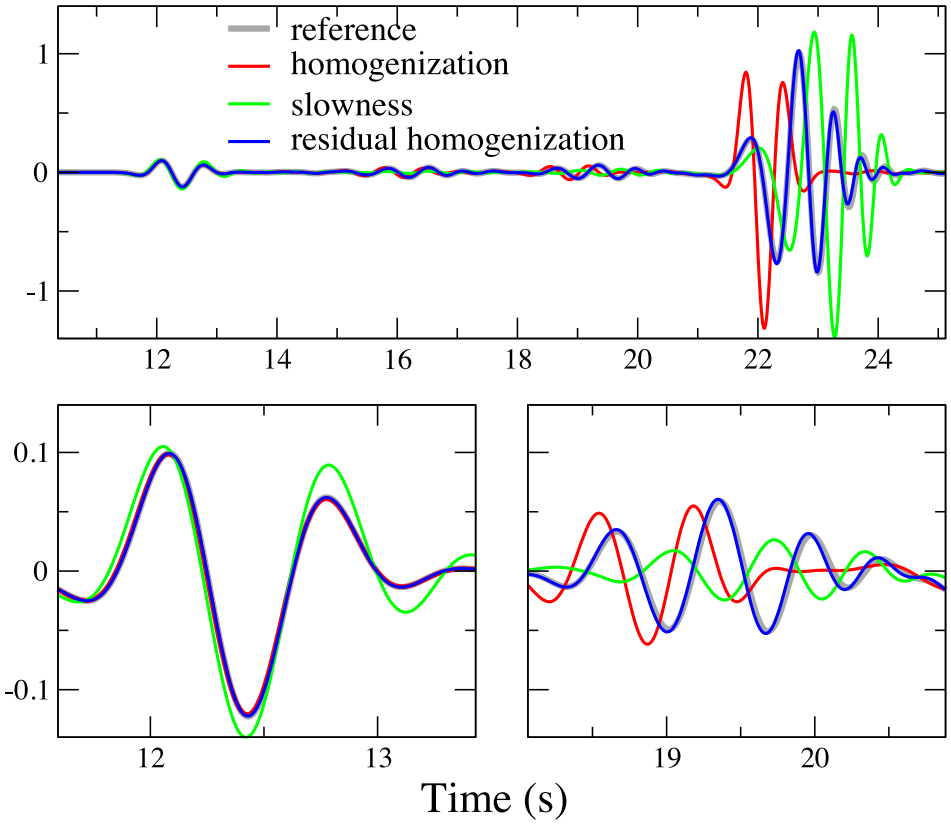

Figure 6. Horizontal displacement recorded at the free surface, 60 km away from the source (diamond symbol in Fig. 2), and computed in the target model ('reference' line), with the classical homogenization ('homogenization' line) with $\varepsilon_0 = 0.5$, in an elastic model obtained by low-pass filtering the slowness ('slowness' line) and with the residual homogenization with $\varepsilon_0 = 0.5$. The top graph shows the signal in the whole time window and the two bottom graphs correspond to two zooms on two different time windows.

the classical homogenization with $\varepsilon_0 = 0.125$ achieve the same accuracy as the residual homogenization with $\varepsilon_0 = 0.4$. Then, despite the necessity to mesh the slow layer, the waveform modelling based on the residual homogenized model is about seven times faster than in the one based on the classical homogenized model (it could be 15 times faster if the mesh generator had placed a single vertical spectral element, instead of two, to mesh the slow shallow layer).

The residual homogenization runs required by themselves only about 3 per cent of the resources necessary to compute the reference solution. For this particular case, the residual homogenization is therefore the best solution.

From this example we see that the residual homogenization, by allowing to homogenize only some specific parts of an elastic model, leaving other parts unchanged, can be an important advantage for forward modelling performances.

4.2 Combining two models of different scale contents

In this section, we present an example where two elastic models with two different scale contents need to be combined. This example is inspired from a potential realistic problem in which a low resolution deterministic model needs to be completed with a high resolution stochastic model. This idea comes from the fact that, on one hand, most tomographic models of the Earth underground contain only the low-frequency response of the real Earth (a low resolution model). On the other hand, it can be of interest to model scattering at high frequency. In general, the high resolution model necessary to model high frequency wavefields is not known and impossible to obtain from classical tomography techniques. The only option left is to rely on a stochastic realization of the elastic properties of the Earth. A good example of a work based on stochastic distributions to generate elastic models can be found in Imperatori & Mai (2013). To study high frequency seismograms in a given region of the Earth, one could be interested in using the known low resolution velocity model of this region and to complete it with a high resolution elastic medium obtained from a stochastic process. This is the purpose of this example: to use a known deterministic low resolution model and to add to it a high wavenumber content from a stochastic distribution.

The whole setting of the following numerical example is a 2-D vertical domain with a free surface at the top. Assuming that we know from a previous study the low resolution elastic model $(\rho^L, \mathbf{c}^L)$ of the domain, for which low frequency synthetic seismograms up to $f^L_{\max} = 0.64$ Hz perfectly fit the data. This model is represented in Figs 11(a) and (c). For the high resolution part, we assume that we only have a statistical idea of the elastic properties of the underground and that a single deterministic realization of the model will be generated according to this statistic. To generate the high resolution model, the band-limited Von Karman correlation function is frequently used in both borehole data analysis (e.g. Holliger 1997; Dolan *et al.* 1998) and numerical simulations (e.g. Frankel & Clayton 1986; Hartzell *et al.* 2010), and adopted also here. Its corresponding power spectrum, in 2-D, is given by:

$$P(k) = \frac{4\pi\sigma^2 a^2 \Gamma(\nu+1)}{\Gamma(\nu)(1+k^2a^2)(\nu+1)}, \tag{26}$$

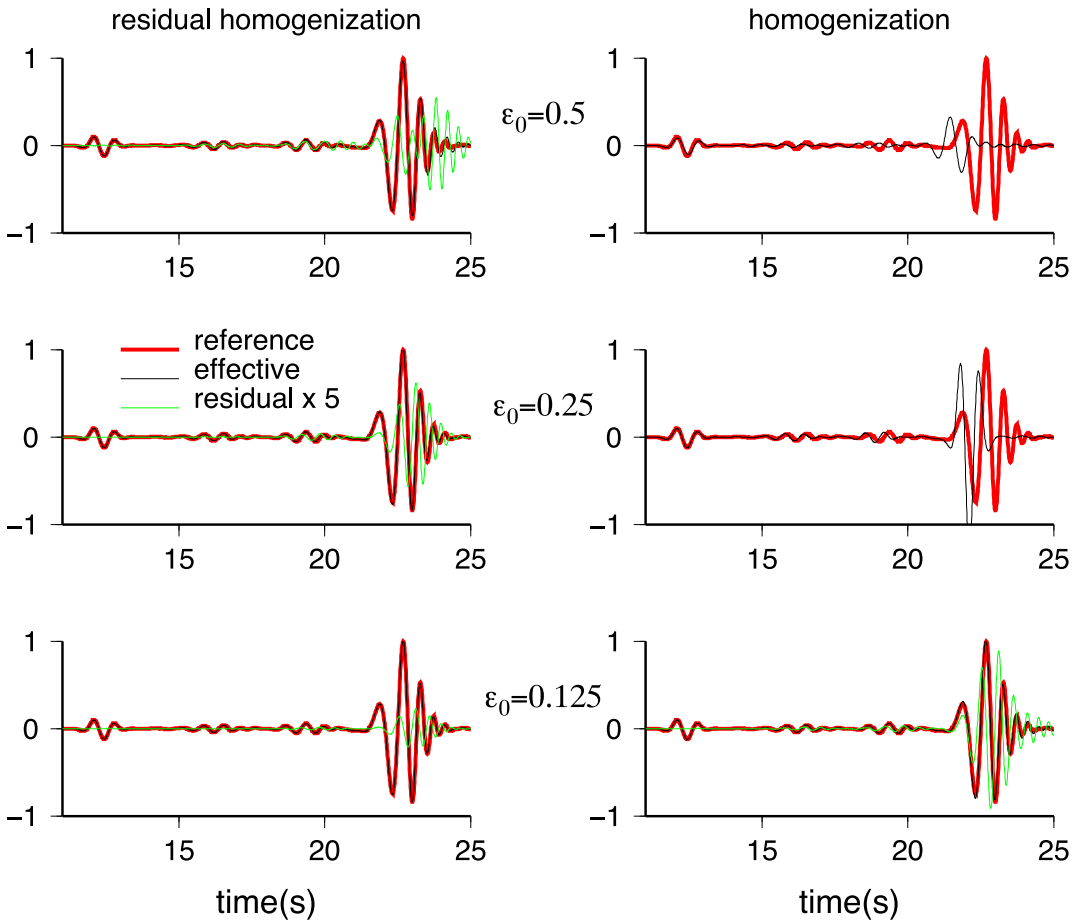

Figure 7. Horizontal displacement recorded at the free surface, 60 km away from the source (diamond symbol in Fig. 2) and computed in the target model ('reference' line), in the homogenized model ('effective' line, right-hand column plots) and in the residual homogenized model ('effective' line, left-hand column plots) for three different values of ε_0. The difference (times 5) between the reference solution and the various solutions is also plotted ('residual × 5' line) when the difference is small.

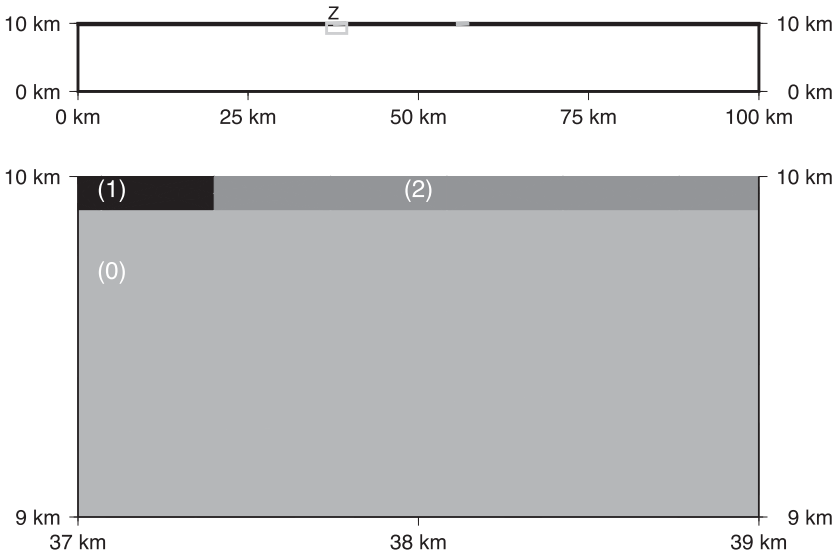

Figure 8. Top panel: sketch describing the reference model used for the residual homogenization test in Section 4.1. The 'Z' rectangle is the zoom area displayed below. Bottom panel: zoom in the 'Z' area. The model is made of three different materials [numbers (0), (1) and (2)] given in Table 1.

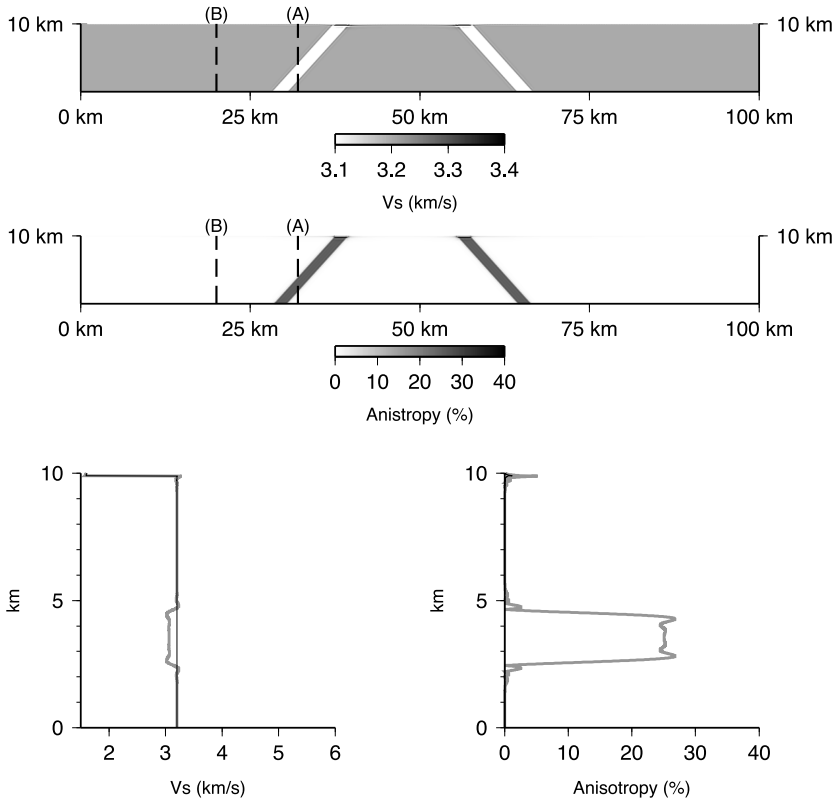

Figure 9. Effective medium obtained by computing the residual homogenization, for $\varepsilon_0 = 0.5$, between the target model shown in Fig. 2 and the reference model presented in Fig. 8. The two top plots show the isotropic V_S and the amount of anisotropy in the effective medium (see text). The two bottom graphs show cross-sections (A) (grey thick lines) and (B) (black thin lies) for the isotropic V_S and the amount of anisotropy measurement in the effective medium.

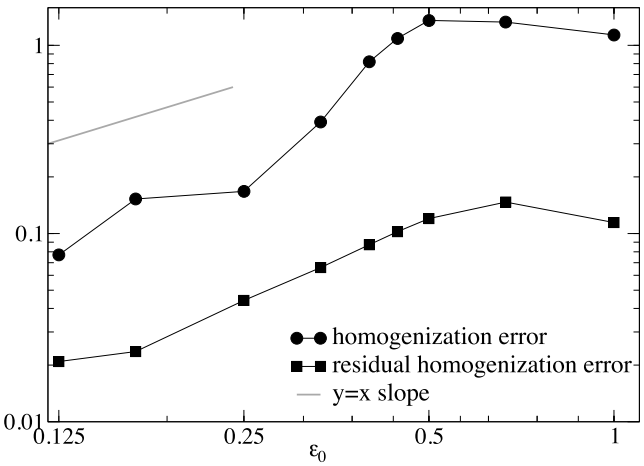

Figure 10. Error $E(\dot{\mathbf{u}}^{\varepsilon_0})$ (see eq. 25) computed for the classical homogenization (black circles) and the residual homogenization (black squares) as a function of ε_0.

where k is the wavenumber, Γ is the Gamma function, σ is the standard deviation, a is the correlation distance and ν is the Hurst exponent which controls the spectral decay at wavenumbers larger than the corner wavenumber ($k > 1/a$). In the literature, the σ, a and ν possible values are poorly constrained. We choose a standard deviation of 10 per cent, a correlation length of 50 m and a Hurst exponent of 0.3. We choose such values because they make it possible to obtain a distribution with a large content of small scales. Such values may not be very realistic but are helping to make our point obvious. To generate a random field $\zeta(\mathbf{x})$ according to the Von Karman distribution, we first generate a random field with a white noise spectrum. This spectrum is filtered with the square root of the Von Karman power spectrum (26) and then Fourier-transformed back to space. An example of given realization is shown in Figs 11(b) and (d). The high resolution elastic model $(\rho^H, \mathbf{c}^H)$ is finally obtained as:

$$\begin{aligned} V_P^H(\mathbf{x}) &= V_P^0[1+\zeta(\mathbf{x})], \\ V_S^H(\mathbf{x}) &= V_S^0[1+\zeta(\mathbf{x})], \\ \rho^H(\mathbf{x}) &= \rho^0[1+\zeta(\mathbf{x})], \end{aligned} \tag{27}$$

where $V_P^0 = 5.8$ km s^{-1}, $V_S^0 = 3.2$ km s^{-1} and $\rho^0 = 3000$ kg m^{-3}.

Having defined the low resolution model $(\rho^L, \mathbf{c}^L)$ and high resolution model $(\rho^H, \mathbf{c}^H)$, the objective is now to combine these two models in a new model. The main constraint is that the combining operation should not change the low frequency response of the elastic model, that is low frequency seismograms computed in this new model must remain unchanged from the ones computed in the deterministic low resolution model $(\rho^L, \mathbf{c}^L)$. Assuming that to the maximum frequency of the low frequency simulation $f^L_{\max}$ corresponds a wavenumber $k^L_{\max}$, a naive way to design this model combining is to introduce a high-pass space filter $\mathbf{I} - \mathcal{F}^{k^L_{\max}}$ and to use it to remove the low wavenumber content of the high resolution model $(\rho^H, \mathbf{c}^H)$ before adding the result to the low resolution model $(\rho^L, \mathbf{c}^L)$:

$$\begin{aligned} \mathbf{c}^{Cn}(\mathbf{x}) &= \mathbf{c}^L(\mathbf{x}) + \left(\mathbf{I} - \mathcal{F}^{k^L_{\max}}\right)(\mathbf{c}^H)(\mathbf{x}), \\ \rho^{Cn}(\mathbf{x}) &= \rho^L(\mathbf{x}) + \left(\mathbf{I} - \mathcal{F}^{k^L_{\max}}\right)(\rho^H)(\mathbf{x}). \end{aligned} \tag{28}$$

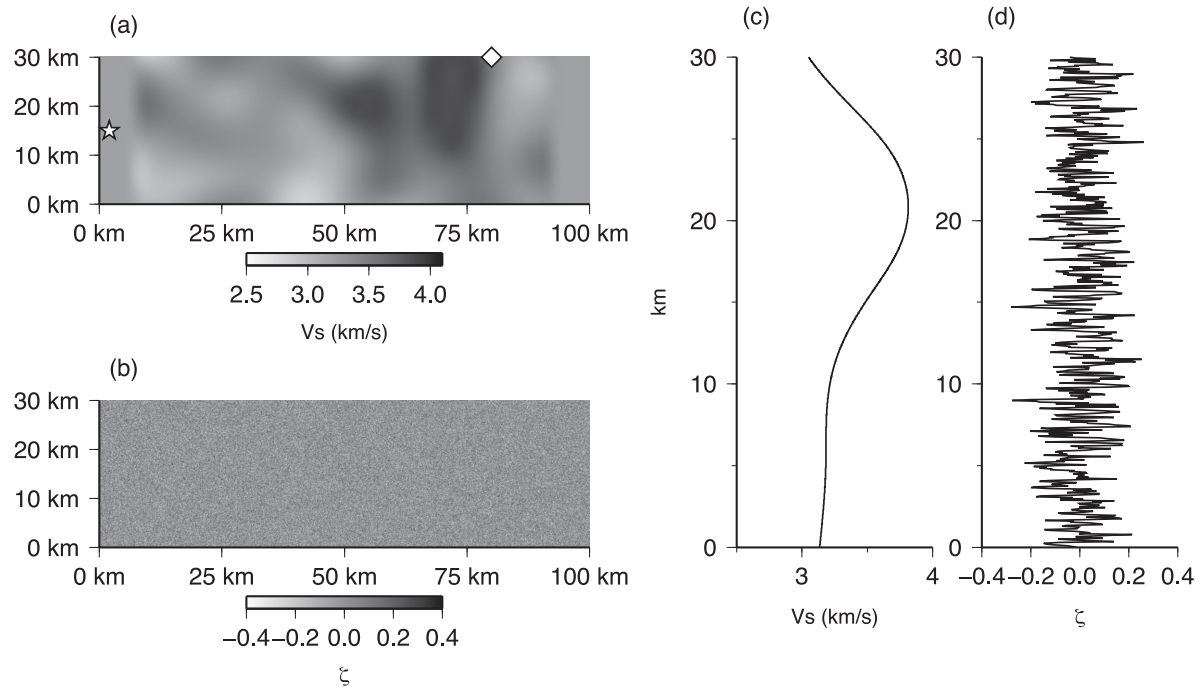

Figure 11. (a) S velocity of the low resolution model. The star symbol indicates the source location and the diamond symbol indicates the receiver location. (b) ζ space function, generated according to the Von Karman power spectrum (26) with a standard deviation of 10 per cent, a correlation length of 50 m and a Hurst exponent of 0.3. (c) vertical cross-section in (a) for $x = 50$ km (x is the horizontal axis). (d) vertical cross-section in (b) for $x = 50$ km.

Doing so, the combined model is left unchanged for low wavenumbers. Nevertheless, as we will see it below, this naive way of combining the models does not satisfy the condition to leave unchanged the low frequency response of the model.

To combine the model properly, we propose a method based on the residual homogenization method. We first solve the cell problem (12) twice, one for $(\rho^L, \mathbf{c}^L)$ and one for $(\rho^H, \mathbf{c}^H)$, to obtain $(\mathbf{G}_{\mathrm{s}}^L, \mathbf{H}_{\mathrm{s}}^L)$ and $(\mathbf{G}_{\mathrm{s}}^H, \mathbf{H}_{\mathrm{s}}^H)$, respectively thanks to (13). The combined initial concentrator tensors are then obtained as:

$$\mathbf{G}_{\mathrm{s}}^C(\mathbf{x}) = \mathbf{G}_{\mathrm{s}}^L(\mathbf{x}) + \left(\mathbf{I} - \mathcal{F}^{k_{\max}^L}\right)\left(\mathbf{G}_{\mathrm{s}}^H\right)(\mathbf{x}),$$

$$\mathbf{H}_{\mathrm{s}}^C(\mathbf{x}) = \mathbf{H}_{\mathrm{s}}^L(\mathbf{x}) + \left(\mathbf{I} - \mathcal{F}^{k_{\max}^L}\right)\left(\mathbf{H}_{\mathrm{s}}^H\right)(\mathbf{x}). \tag{29}$$

Finally, the homogenized combined model is obtained as:

$$\mathbf{c}^{Ch}(\mathbf{x}) = \mathbf{H}_{\mathrm{s}}^C : \left(\mathbf{G}_{\mathrm{s}}^C\right)^{-1}(\mathbf{x}),$$

$$\rho^{Ch}(\mathbf{x}) = \rho^L(\mathbf{x}) + \left(\mathbf{I} - \mathcal{F}^{k_{\max}^L}\right)\left(\rho^H\right)(\mathbf{x}). \tag{30}$$

Fig. 12 shows the homogenized model S velocity and two vertical cross-sections, one in the model combined according to the residual homogenization method (30) and the other according to the naive method (28). If the two cross-sections display some common features, they also show significant differences.

Fig. 13 shows the vertical component seismograms, recorded at the free surface, 80 km away from the source, and computed in the low resolution model $(\rho^L, \mathbf{c}^L)$, in the residual homogenization combined model $(\rho^{Ch}, \mathbf{c}^{Ch})$ and in the naive combined model $(\rho^{Cn}, \mathbf{c}^{Cn})$. As it can be seen the seismogram computed in the naive combined model does not match the reference seismogram computed in the low frequency model. They display a phase delay and a different coda waveform. This implies that the naive combining operation has changed the low frequency response of the model,

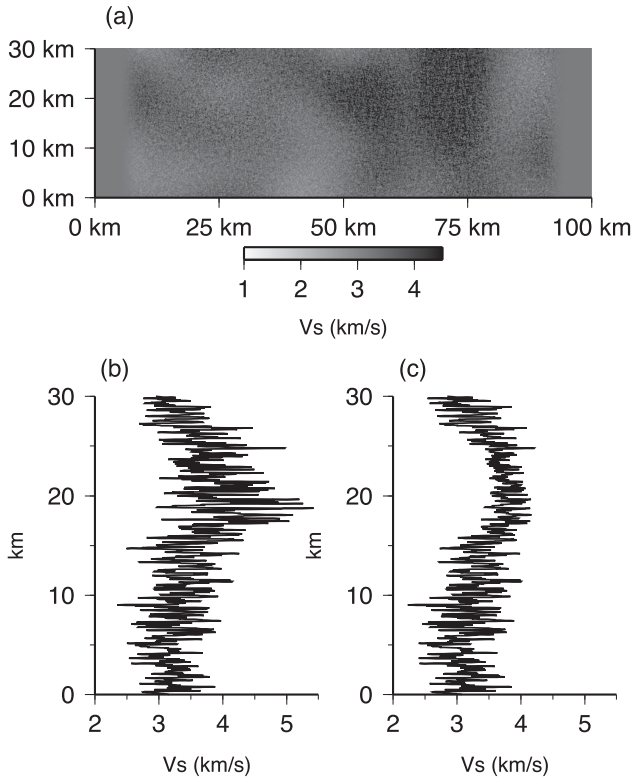

Figure 12. (a) S velocity of the combined model using the residual homogenization method (30). (b) Vertical cross-section for the residual homogenized combined model (based on eq. 30) for $x = 50$ km. (c) Vertical cross-section for the naive combined model (based on eq. 28) for $x = 50$ km.

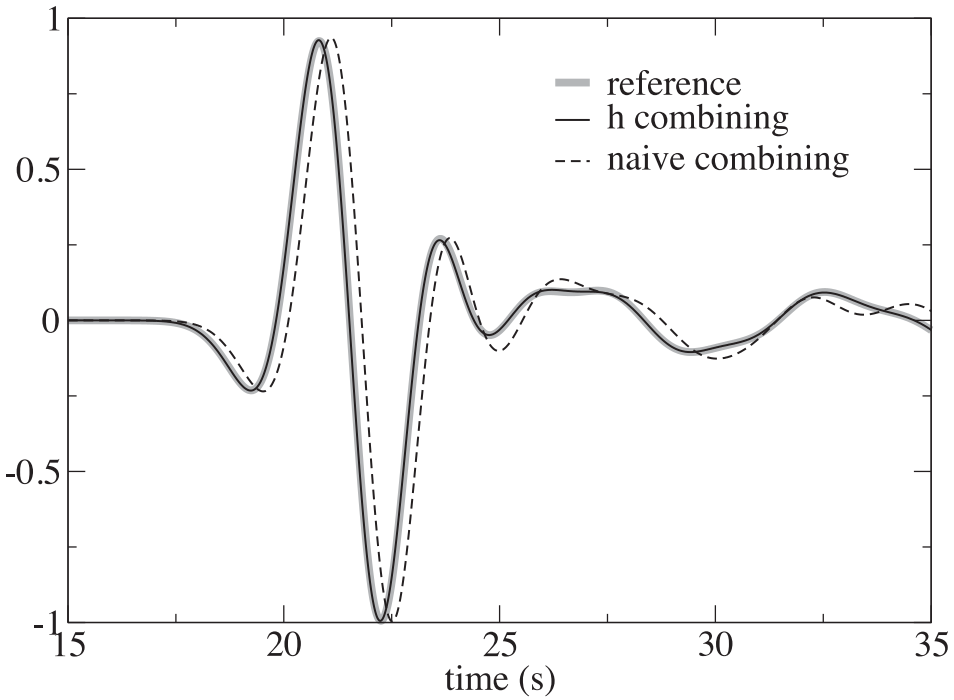

Figure 13. Low frequency vertical component seismograms recorded at the free surface, 60 km away from the source (diamond symbol in Fig. 11) computed in the low resolution model (ρ^L, $\mathbf{c}^L$) ('reference' line), in the residual homogenized combined model (ρ^{Ch}, $\mathbf{c}^{Ch}$) ('h combined' line) and in the naive combined model (ρ^{Cn}, $\mathbf{c}^{Cn}$) ('naive combined' line).

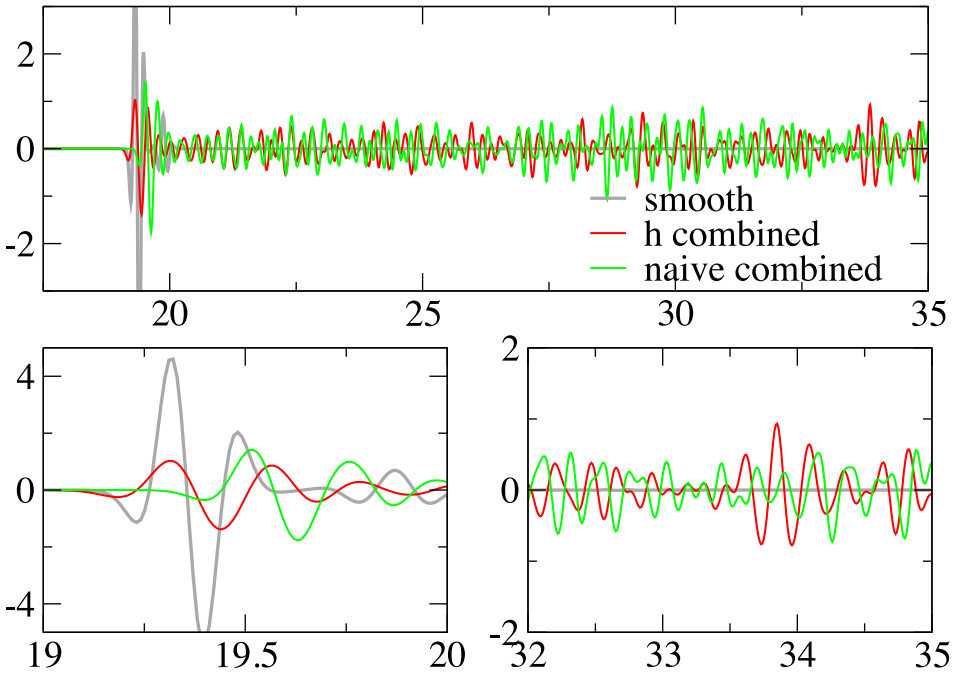

Figure 14. Top graph: high frequency vertical component seismograms recorded at the free surface, 60 km away from the source (diamond symbol in Fig. 11) and computed in the low resolution model (ρ^L, $\mathbf{c}^L$) ('reference' line), in the residual homogenized combined model (ρ^{Ch}, $\mathbf{c}^{Ch}$) ('h combined' line) and in the naive combined model (ρ^{Cn}, $\mathbf{c}^{Cn}$) ('naive combined' line). Bottom graphs: zooms in two different time windows of the top graph seismograms.

which we wanted to avoid. On the other hand, the seismogram computed in the model combined with the residual homogenization method match perfectly the reference seismogram, implying that the residual homogenization method is able to 'add' a high wavenumber content to the low resolution model without changing its low frequency response, which was our main objective for this example.

Fig. 14 shows seismograms recorded in the same configuration as for Fig. 13, but this time for a high frequency content: $f_{\max} \simeq 11.5$ Hz. On one hand, as expected, the seismogram computed in the low resolution model shows only a clear direct arrival with no coda: the model is too smooth to make it possible for diffraction to be significant. On the other hand, the two seismograms computed in the naive and residual homogenization combined models show

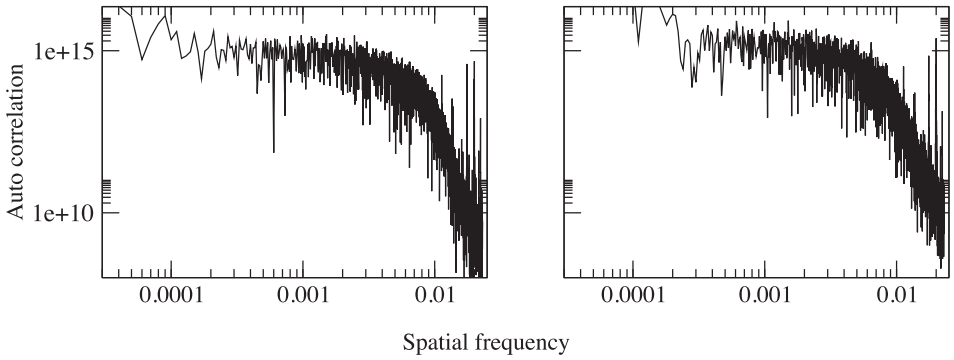

Figure 15. Autocorrelation power spectrum computed for $c_{1111}(\mathbf{x})$ in the naive homogenized model (left-hand plot) and in the residual homogenized model (right-hand plot).

a very strong diffraction coda, but they are significantly different from each other.

In conclusion, the residual homogenization can help to combine low resolution and high resolution elastic models in a consistent way. This example is a demonstration test and not a beginning of study similar to the one presented by Imperatori & Mai (2013). Nevertheless, this example raises questions on the way elastic models should be generated from stochastic distributions. In particular, we may wonder how the different ways to combine models may impact the final power spectrum of the elastic parameters? A quick check on the autocorrelation functions of one particular elastic coefficient (c_{1111}) is presented in Fig. 15 for the naive and residual homogenized combined models. If the two plots display some differences, they are also very similar. Does that mean that the way we combine the models does not significantly impact the final model power spectrum? We do not try to address this question here, but the way elastic models are built and combined from stochastic distributions should be studied, in a future work, from the residual homogenization perspective.

5 CONCLUSION

We have presented an extension to the non-periodic homogenization method allowing to homogenize the difference, or residual, between two media. This extension can be useful in various situations. For example, it allows to compute an effective medium only where the reference and the target models are different, making it possible to homogenize only some parts of the elastic model or to keep some interfaces from the target model in the homogenized model. As shown in the given example, if this extension does not change the convergence rate with ε_0 of the asymptotic two scale approximation, it can help to minimize the constant factor of the convergence and seriously minimize the error of the method. The method can also allow to combine properly two elastic models with different scale contents. Finally, the main application may be the full waveform inverse problem: as it has been numerically shown in the layered case (Capdeville *et al.* 2013), we postulate that a model obtained from a full waveform inverse problem based on seismic data in a limited frequency band is, at best, the residual homogenized model between the real model and the reference model used for the inversion. However this remains to be shown for 2-D and 3-D problems and will be the subject of a future work.

ACKNOWLEDGEMENTS

This work was funded by the ANR blanche ‘mémé’ grant (ANR-10-BLAN-613 MEME). Computations were performed on the CCIPL computer ‘Erdre’. We thank Gaetano Festa for letting us use and modify his 2-D spectral element program. We thank Andreas Fichtner and Wolfgang Friedrich for their helpful reviews.

REFERENCES

Backus, G., 1962. Long-wave elastic anisotropy produced by horizontal layering, *J. geophys. Res.,* **67**(11), 4427–4440.

Browaeys, J.T. & Chevrot, S., 2004. Decomposition of the elastic tensor and geophysical applications, *Geophys. J. Int.,* **159,** 667–678.

Capdeville, Y. & Marigo, J.J., 2007. Second order homogenization of the elastic wave equation for non-periodic layered media, *Geophys. J. Int.,* **170,** 823–838.

Capdeville, Y. & Marigo, J.J., 2008. Shallow layer correction for spectral element like methods, *Geophys. J. Int.,* **172,** 1135–1150.

Capdeville, Y. & Marigo, J.-J., 2013. A non-periodic two scale asymptotic method to take account of rough topographies for 2-D elastic wave propagation, *Geophys. J. Int.,* **192**(1), 163–189.

Capdeville, Y., Guillot, L. & Marigo, J.J., 2010a. 1-D non periodic homogenization for the wave equation, *Geophys. J. Int.,* **181,** 897–910.

Capdeville, Y., Guillot, L. & Marigo, J.J., 2010b. 2-D non-periodic homogenization to upscale elastic media for P-SV waves, *Geophys. J. Int.,* **182,** 903–922.

Capdeville, Y., Stutzmann, É., Wang, N. & Montagner, J.-P., 2013. Residual homogenization for seismic forward and inverse problems in layered media, *Geophys. J. Int.,* **194**(1), 470–487.

Capdeville, Y., Zhao, M. & Cupillard, P., 2014. Fast fourier homogenization for elastic wave propagation in complex media, *Wave Motion,* in press.

Chaljub, E., Komatitsch, D., Capdeville, Y., Vilotte, J.-P., Valette, B. & Festa, G., 2007. Spectral element analysis in seismology, in *Advances in Wave Propagation in Heterogeneous Media,* Vol. 48, pp. 365–419, eds Wu, R.-S. & Maupin, V., Advances in Geophysics Series, Elsevier.

Dolan, S.S., Bean, C.J. & Riollet, B., 1998. The broad-band fractal nature of heterogeneity in the upper crust from petrophysical logs, *Geophys. J. Int.,* **132**(3), 489–507.

Festa, G. & Vilotte, J.-P., 2005. The newmark scheme as velocity-stress time-staggering: an efficient implementation for spectral element simulations of elastodynamics, *Geophys. J. Int.,* **161,** 789–812.

Fichtner, A. & Igel, H., 2008. Efficient numerical surface wave propagation through the optimization of discrete crustal models—a technique based on non-linear dispersion curve matching (DCM), *Geophys. J. Int.,* **173**(2), 519–533.

Fichtner, A., Trampert, J., Cupillard, P., Saygin, E., Taymaz, T., Capdeville, Y. & Villaseñor, A., 2013. Multiscale full waveform inversion, *Geophys. J. Int.,* **194**(1), 534–556.

Frankel, A. & Clayton, R.W., 1986. Finite difference simulations of seismic scattering: implications for the propagation of short-period seismic waves in the crust and models of crustal heterogeneity, *J. geophys. Res.,* **91**(B6), 6465–6489.

Geuzaine, C. & Remacle, J.-F., 2009. Gmsh: a three-dimensional finite element mesh generator with built-in pre- and post-processing facilities, *Int. J. Num. Methods Eng.,* **79,** 1309–1331.

Guillot, L., Capdeville, Y. & Marigo, J.J., 2010. 2-D non periodic homogenization for the SH wave equation, *Geophys. J. Int.,* **182,** 1438–1454.

Hartzell, S., Harmsen, S. & Frankel, A., 2010. Effects of 3d random correlated velocity perturbations on predicted ground motions, *Bull. seism. Soc. Am.,* **100**(4), 1415–1426.

Holliger, K., 1997. Seismic scattering in the upper crystalline crust based on evidence from sonic logs, *Geophys. J. Int.,* **128**(1), 65–72.

Imperatori, W. & Mai, P., 2013. Broad-band near-field ground motion simulations in 3-dimensional scattering media, *Geophys. J. Int.,* **192**(2), 725–744.

Komatitsch, D. & Vilotte, J.P., 1998. The spectral element method: an effective tool to simulate the seismic response of 2D and 3D geological structures, *Bull. seism. Soc. Am.,* **88,** 368–392.

Lekić, V., Panning, M. & Romanowicz, B., 2010. A simple method for improving crustal corrections in waveform tomography, *Geophys. J. Int.,* **182**(1), 265–278.

Sanchez-Palencia, E., 1980. *Non Homogeneous Media and Vibration Theory,* Number 127 in Lecture Notes in Physics, Springer.

Suquet, P., 1982. Plasticité et homogénéisation, *Thèse d'Etat*. Université Pierre et Marie Curie, Paris.

Takeuchi, H. & Saito, M., 1972. Seismic surface waves, *Methods Computat. Phys.,* **11,** 217–295.